

Finite-Difference Time-Domain Simulation of the Maxwell–Schrödinger System

Christopher Jayun Ryu, Aiyin Y. Liu, Wei E. I. Sha, *Member, IEEE*, and Weng Cho Chew, *Fellow, IEEE*

Abstract—A thorough study on the finite-difference time-domain (FDTD) simulation of the Maxwell–Schrödinger system in the semiclassical regime is given. For the Maxwell part which is treated classically, this novel approach directly using the vector and scalar potentials (\mathbf{A} and Φ) is taken. This approach is stable in the long-wavelength regime and removes the need to extract the potentials at every time step. The perfectly matched layer important for FDTD simulations is developed for this new approach. For the Schrödinger and quantum mechanical part, minimal coupling is applied to couple the charges to the electromagnetic potentials. FDTD stability is analyzed for the whole system and simulation results agree with the properties of quantum coherent states.

Index Terms—Maxwell–Schrödinger, nanophotonics, quantum-dots.

I. INTRODUCTION

RECENT advances in nanotechnology have shrunk the length scales of electronic devices down to nanometers which are much smaller compared to optical wavelengths. Due to this miniaturization, the quantum nature of charges becomes more pronounced in the electronic devices. The system of charge plus field needs to be modeled quantum mechanically. While a fully quantum mechanical picture would also have the field quantized, there is still a large application area for models where the field is treated classically. This is termed as the semiclassical regime, in which the classical Maxwell's equations for the field is coupled to the quantum mechanical Schrödinger equation for the charged particle [1].

In this paper, we work with the Maxwell–Schrödinger system in time domain, where the dynamics of the coupled system can be time stepped using the finite-difference time-domain (FDTD) method. FDTD has been used to study this system for nearly two decades. Two schools of formulations are popular. When the interactions are nearly resonant, the physics can be approximated as restricted to several bound states of the electron. This allows

for the projection of the Schrödinger part into a subspace, in which one solves the Maxwell–Bloch equations or the quantum Liouville equations for the density matrix [1]. This method has been applied to the study of ultrafast optical pulse simulations [2], excitonics in quantum dots [3], nanoplasmonics [4], and nanopolaritonics [5], [6]. Furthermore, loss mechanisms can be incorporated into the system by a combined Maxwell–Bloch Langevin approach [4].

The other school of formulations, however, retains the wavefunction in its entirety. This work belongs to the latter school. One of the first works involved a straightforward three-dimensional FDTD scheme to simulate a single electron tunneling problem [7]. More recent study discusses the control of particle quantum states using optimal laser pulses designed through the Maxwell–Schrödinger simulations [8]. Since the Schrödinger equation couples directly to the magnetic vector potential (\mathbf{A}) and the electric scalar potential (Φ), rather than the electric and magnetic fields (\mathbf{E} and \mathbf{H}), these simulations require the extraction of \mathbf{A} and Φ at every time step [7], [9]. This can be avoided through the use of gauge transformations, after which the Schrödinger equation couples directly to the fields. The length gauge was applied for this purpose in [10]. However, a long wavelength approximation is inherent in the length gauge, thus limiting its applicability.

It should be noted that for some of the aforementioned systems, simulations in which the quantum dots are further simplified into polarization densities [11] or effective permittivity models [12], [13] suffice to describe the essential features. However, we choose to couple the Maxwell–Schrödinger equations directly in the spirit that the simulation should come from the first principle as much as possible.

It is well known that in the long wavelength, conventional Maxwell's equations suffer from low frequency breakdown due to the imbalance of frequency scaling. This was previously overlooked in the Maxwell–Schrödinger system. In view of these, we developed a new FDTD scheme. For the Maxwell part, the \mathbf{A} - Φ formulation [14] is used and the potentials are directly time stepped. With this, the extraction of potentials, the approximation of the length gauge as well as low-frequency instability are avoided.

In Section II, FDTD simulation under the \mathbf{A} - Φ formulation is discussed. Perfectly matched layer (PML) is formulated for the simulation of open problems. In Section III, FDTD of the coupled \mathbf{A} - Φ equations and Schrödinger equation is discussed. In Section IV, the simulation is applied to study an electron trapped in a quadratic potential under plane wave excitation. This is a simple model for a quantum dot interacting with light, a problem that had been studied extensively using the FDTD technique but with a semiclassical dipole model for the quantum dot [11]. Physics of coherent states are reproduced in accordance with the expected behavior of a quantum harmonic oscillator.

Manuscript received February 20, 2016; revised May 24, 2016; accepted July 14, 2016. Date of publication September 1, 2016; date of current version October 19, 2016. This work was supported in part by the USA NSF CCF Award 1218552, in part by the National Natural Science Foundation of China under Grant 61201122, and in part by the Seed Fund of University of Hong Kong under Grant 201411159192.

C. J. Ryu is with the Department of Electrical and Computer Engineering, University of Illinois at Urbana-Champaign, Champaign, IL 61820 USA, on leave from the Department of Electrical Communication Engineering, University of Illinois at Urbana-Champaign, Champaign, IL 61820 USA (e-mail: chrisjayunryu@gmail.com).

A. Y. Liu and W. C. Chew are with the Department of Electrical and Computer Engineering, University of Illinois at Urbana-Champaign, Champaign, IL 61820 USA (e-mail: liu141@illinois.edu; w-chew@uiuc.edu).

W. E. I. Sha is with the Department of Electrical and Electronic Engineering, University of Hong Kong, Hong Kong (e-mail: wsha@eee.hku.hk).

Color versions of one or more of the figures in this paper are available online at <http://ieeexplore.ieee.org>.

Digital Object Identifier 10.1109/JMMCT.2016.2605378

Finally, we conclude this work and discuss directions for future work in Section V.

II. FDTD FORMULATION OF MAXWELL'S EQUATIONS

The \mathbf{A} - Φ formulation is an effective alternative to conventional Maxwell's equations due to its stability in the long wavelength regime [14] and the fact that the potentials directly enter into the Schrödinger equation instead of the fields. The equations for the \mathbf{A} - Φ formulation are discretized, and the application of the coordinate stretching PML is shown.

The potentials are related to the electric and magnetic field through

$$\mathbf{B} = \nabla \times \mathbf{A} \quad (1)$$

$$\mathbf{E} = -\frac{\partial}{\partial t} \mathbf{A} - \nabla \Phi. \quad (2)$$

From these relations and Maxwell's equations in inhomogeneous isotropic media, the equations for the \mathbf{A} - Φ formulation can be derived as in [14]. They are written as

$$\nabla \cdot \epsilon \nabla \Phi - \epsilon^2 \mu \frac{\partial^2}{\partial t^2} \Phi = -\rho \quad (3)$$

$$-\nabla \times \mu^{-1} \nabla \times \mathbf{A} - \epsilon \frac{\partial^2}{\partial t^2} \mathbf{A} + \epsilon \nabla \epsilon^{-2} \mu^{-1} \nabla \cdot \epsilon \mathbf{A} = -\mathbf{J}. \quad (4)$$

They are under the generalized Lorenz gauge

$$\epsilon^{-1} \nabla \cdot \epsilon \mathbf{A} = -\mu \epsilon \frac{\partial \rho}{\partial t}. \quad (5)$$

This gauge has the physical significance that the formulation remains relativistic in vacuum. We take it to be the natural gauge condition in inhomogeneous media. The two sources in the \mathbf{A} - Φ equations are related by the current continuity equation

$$\nabla \cdot \mathbf{J} + \frac{\partial \rho}{\partial t} = 0. \quad (6)$$

A. Discretization

In order to discretize (3) and (4), the discrete electromagnetic (EM) theory on a lattice [15] will be applied, and this theory is consistent with the widely known Yee's grid [16]. A brief review of the discrete vector calculus from the discrete EM theory can be found in Appendix A

$$\begin{aligned} \hat{\nabla} \times \mu_{\mathbf{m}+1/2}^{-1} \tilde{\nabla} \times \tilde{\mathbf{A}}_{\mathbf{m}}^{n-1/2} + \epsilon_{\mathbf{m}} \tilde{\partial}_t \hat{\partial}_t \tilde{\mathbf{A}}_{\mathbf{m}}^{n-1/2} \\ - \epsilon_{\mathbf{m}} \tilde{\nabla} \mu_{\mathbf{m}}^{-1} \epsilon_{\mathbf{m}}^{-2} \hat{\nabla} \cdot \epsilon_{\mathbf{m}} \tilde{\mathbf{A}}_{\mathbf{m}}^{n-1/2} = \tilde{\mathbf{J}}_{\mathbf{m}}^{n-1/2} \end{aligned} \quad (7)$$

$$-\hat{\nabla} \cdot \epsilon_{\mathbf{m}} \tilde{\nabla} \Phi_{\mathbf{m}}^n + \mu_{\mathbf{m}} \epsilon_{\mathbf{m}}^2 \tilde{\partial}_t \hat{\partial}_t \Phi_{\mathbf{m}}^n = \rho_{\mathbf{m}}^n \quad (8)$$

$$\hat{\nabla} \cdot \tilde{\mathbf{J}}_{\mathbf{m}}^{n-1/2} + \hat{\partial}_t \rho_{\mathbf{m}}^n = 0. \quad (9)$$

The discretized \mathbf{A} - Φ equations are shown as (7)–(9). Here, the primary and dual grids are indexed by $\mathbf{m} = (i, j, k)$ and $\mathbf{m} + 1/2 = (i + 1/2, j + 1/2, k + 1/2)$, respectively. The chosen discretization scheme arranges forward and backward differencing so that all derivatives are central. Hence, the FDTD simulation of the field part is second-order accurate. The time stepping equations are given in (25) through (27) in Appendix A.

The stability condition for these equations is the same as the FDTD stability condition for Maxwell's equations [17]

$$\Delta t \leq \frac{1}{c \sqrt{\frac{1}{\Delta x^2} + \frac{1}{\Delta y^2} + \frac{1}{\Delta z^2}}}. \quad (10)$$

B. Perfectly Matched Layers

As often employed in the FDTD simulation of Maxwell's equations, the Dirichlet boundary conditions are applied at the boundaries of the simulation domain. In order to efficiently simulate an infinite space, PML must be developed for the \mathbf{A} - Φ equations. A very simple way of implementing PML using the idea of coordinate stretching was first introduced in [18]. This same technique can be applied to implement PML for the \mathbf{A} - Φ equations. We relegate the details of the implementation to Appendix B.

III. MAXWELL–SCHRÖDINGER SYSTEM

The \mathbf{A} - Φ potentials enter the Schrödinger equation through the minimal coupling Hamiltonian [1]. In the semiclassical picture, we model the back action of the particle on the field by interpreting the probability current as a radiation source.

A. Governing Equations

From the minimal coupling Hamiltonian, the time-dependent Schrödinger equation is written as

$$\begin{aligned} i\hbar \frac{\partial}{\partial t} \psi(\mathbf{r}, t) = \frac{1}{2m^*} \left(\frac{\hbar}{i} \nabla - q\mathbf{A} \right)^2 \psi(\mathbf{r}, t) + \Phi(\mathbf{r}, t) \psi(\mathbf{r}, t) \\ + V(\mathbf{r}, t) \psi(\mathbf{r}, t) \end{aligned} \quad (11)$$

where $\hbar = \frac{h}{2\pi}$, h is the Planck constant, ψ is the wavefunction of the particle where $|\psi|^2$ represents the probability density function of the particle, m^* is the effective mass of the particle, and V is the confinement potential. To establish the back action of the particle on the field, we replace the charge and current in (3) and (4) with their quantum mechanical analogs ρ_q and \mathbf{J}_q , denoted with a subscript q to indicate their quantum nature. These sources obey the continuity equation for probability amplitude

$$\nabla \cdot \mathbf{J}_q + \frac{\partial \rho_q}{\partial t} = 0. \quad (12)$$

They are calculated instantaneously from the wavefunction as [19]

$$\mathbf{J}_q = \frac{q}{2} \left\{ \left[\frac{\hat{p} - q\mathbf{A}}{m^*} \psi \right]^* \psi + \psi^* \left[\frac{\hat{p} - q\mathbf{A}}{m^*} \psi \right] \right\} \quad (13)$$

$$\rho_q = q |\psi(\mathbf{r}, t)|^2. \quad (14)$$

Here, $\hat{p} = \frac{\hbar}{i} \nabla$ is the momentum operator.

Two points should be noted in connection with the fully quantized theory. First, the \mathbf{J}_q in (13) comes from tracing the symmetric particle current operator over the field states. Second, the \mathbf{A}^2 term captures the physics of plasma oscillations of the electron in the field. Although its effects are not pronounced in the simulation scheme of Section IV due to the small charge and low field intensity, it is expected to be of importance when field intensities are high, such as in nanoplasmonic applications. The link between the semiclassical and fully quantized

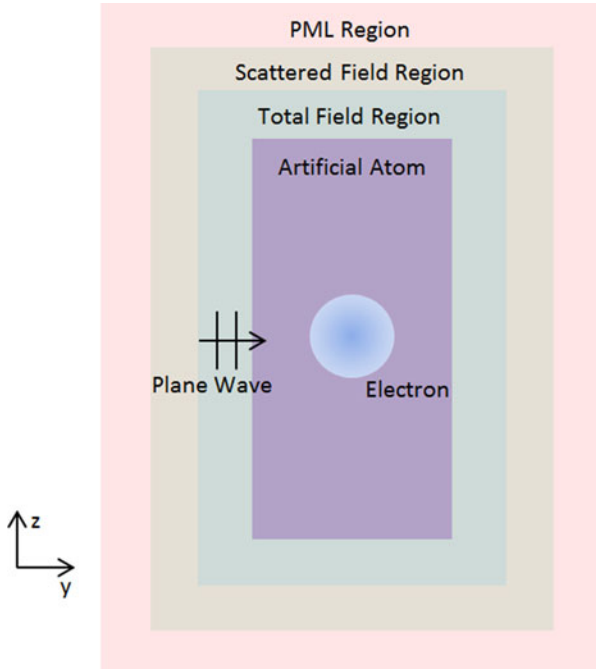


Fig. 1. Illustration of the simulation setting for an artificial atom.

theory is the restriction that the field states be coherent, and not entangled with the electron state. The discretization of the modified Schrödinger equation and the particle current are shown in Appendix C.

B. Stability Condition

The time-step, Δt , is taken to be the minimum of the two from the \mathbf{A} - Φ equations or the Schrödinger equation. The time-step for the \mathbf{A} - Φ equations has been shown, and the one for the Schrödinger equation has been presented in other papers [20]. We modify it here and show the result in (15) are shown at the bottom of the page. Note that when the field is turned OFF, we recover the stability condition for the simple Schrödinger equation, see (15) shown at the bottom of the page.

IV. SIMULATION RESULTS

The Maxwell–Schrödinger system is used, for example, to simulate a single electron trapped in an artificial atom (quantum dot). The effective mass Schrödinger equation can be used to simulate many electrons problem with a single electron. The electron can be trapped by a potential or quantum well generated by a heterogeneous (heterojunction) materials, or by a defect in a crystal lattice. For simplicity, the confinement potential of the atom is characterized by a harmonic oscillator. The simulation setting is illustrated in Fig. 1. This setting mimics the quantum dot introduced in [21]. The effective mass of the electron is $m^* = 0.023m_0$, where m_0 is the electron rest mass, and the angular frequency of the harmonic oscillator is $\omega = \frac{2\pi c}{\lambda}$, where $\lambda =$

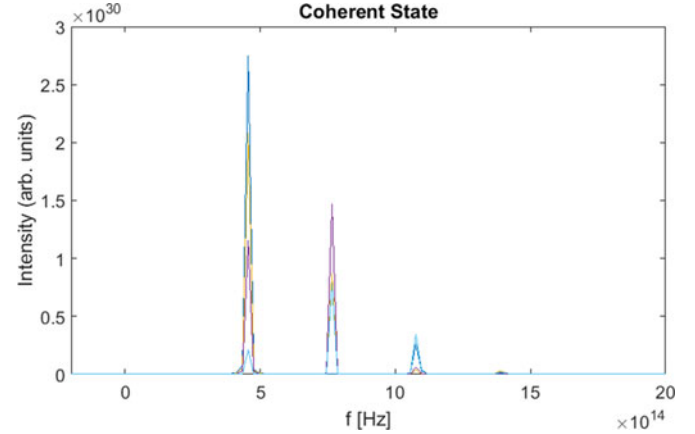


Fig. 2. Plot of eigenenergy levels of a simulated coherent state.

950 nm. The electron is initialized in the ground state. The plane wave is given by $\mathbf{A}^{\text{inc}} = \hat{z}1.4871 \times 10^{-7} \sin(ky - \omega t)$ V · s/m or $\mathbf{E}^{\text{inc}} = -\hat{z}2.9487 \times 10^8 \cos(ky - \omega t)$ V/m which corresponds to an average number of six photons in the simulation space. The simulation domain is narrow in x - and y -directions to reduce the number of unknowns and the simulation time.

The state of a harmonic oscillator driven by a classical field is called a coherent state. The expression for a coherent state is given by [22]

$$|z\rangle = e^{-\frac{|z|^2}{2}} \sum_{n=0}^{\infty} \frac{z^n}{\sqrt{n!}} |n\rangle \quad (16)$$

where $z = \sqrt{E_0} e^{i\varphi(t)}$, n is the mode number in the harmonic oscillator, E_0 is the average number of photons in the mode, and $\varphi(t)$ is a real function in time that represents the phase of the state. The probability of finding mode n in this coherent state is

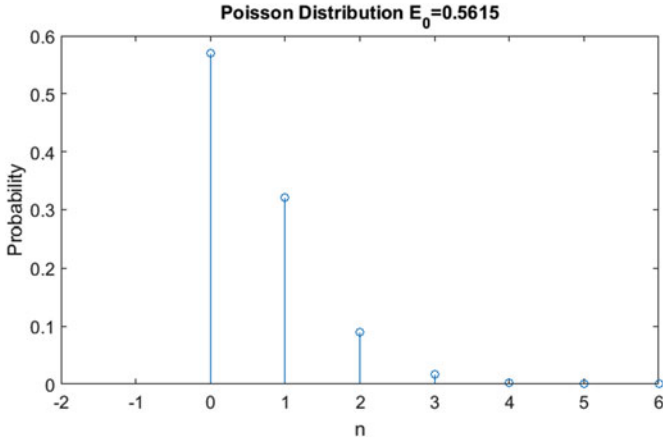
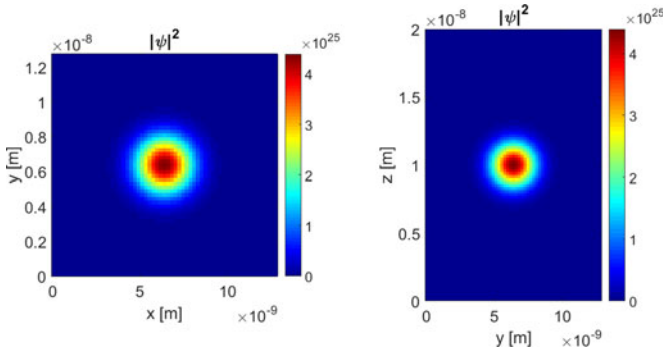
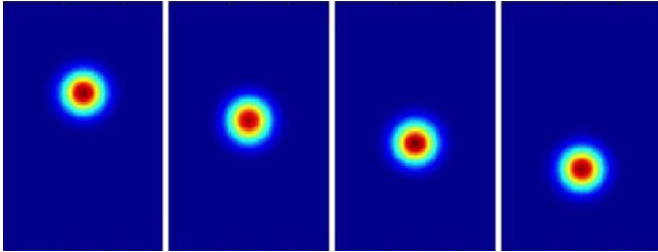
$$p_n(z) = \frac{E_0^n}{n!} e^{-E_0} \quad (17)$$

which is a Poisson distribution.

For the excitation of the coherent state, the electron is excited initially by a classical plane wave, and then the technique described in [23] is used to map out the distribution of eigenstates in the electron's wavefunction. In Fig. 2, the overlapped distribution of eigenstates at several observation points (represented by different colors) is shown to match the Poisson distribution as the theory suggests. Due to the spatial dependence of the eigenstates of a harmonic oscillator, the Poisson distribution is not reflected at every observation point. Note that the eigenfrequencies are all equidistant, which is characteristic of a quantum harmonic oscillator. We see that mainly three modes are excited by the plane wave, and the peak is located at $n = 0$. In order to find the Poisson distribution with the peak at the same location, derivative of (17) is taken

$$\frac{d}{dn} p_n(z) = \frac{E_0^n (\ln E_0 - \psi^{(0)}(n+1))}{e^{E_0} \Gamma(n+1)} \quad (18)$$

$$\Delta t \leq \frac{\hbar}{\frac{1}{m^*} \left[4\hbar^2 \left(\frac{1}{\Delta x^2} + \frac{1}{\Delta y^2} + \frac{1}{\Delta z^2} \right) - 2\hbar q \left(\frac{A_x}{\Delta x} + \frac{A_y}{\Delta y} + \frac{A_z}{\Delta z} \right) + q^2 |\mathbf{A}|^2 \right] + V_{\max}} \quad (19)$$


 Fig. 3. Plot of the Poisson distribution with $E_0 = 0.5615$ photons.

 Fig. 4. Plots of xy - and yz -plane slices of an electron in a ground state in an artificial atom with the quadratic confinement potential.

 Fig. 5. Snapshots of yz -plane slices at different time steps. The electron is in a coherent state after it has been excited by light.

where $\psi^{(m)}(z)$ is the polygamma function of order m and $\Gamma(n)$ is the gamma function. To find a Poisson distribution with a peak located at $n = 0$, we let the above derivative be equal to zero and find the value of E_0 . It is found to be $E_0 = 0.5615$ photons. The corresponding Poisson distribution is plotted in Fig. 3.

In the simulation space, the average number of photons was set to be six photons, and this indicates that the electron absorbed $\frac{E_0}{6} \times 100 \approx 9.36\%$ of the photons in space. In terms of volume, this corresponds to a sphere with a radius of 4.1758 nm, and most of the probability density of the electron is contained in this sphere. As a reference, a plot of the electron in the ground state is shown in Fig. 4. In contrast, Fig. 5 shows the electron after it has been excited by the plane wave. It shows the movement of the electron in the z -direction swinging back and forth.

If the number of photons in the simulation space is tripled from 6 to 18, then E_0 is also expected to triple from the previ-

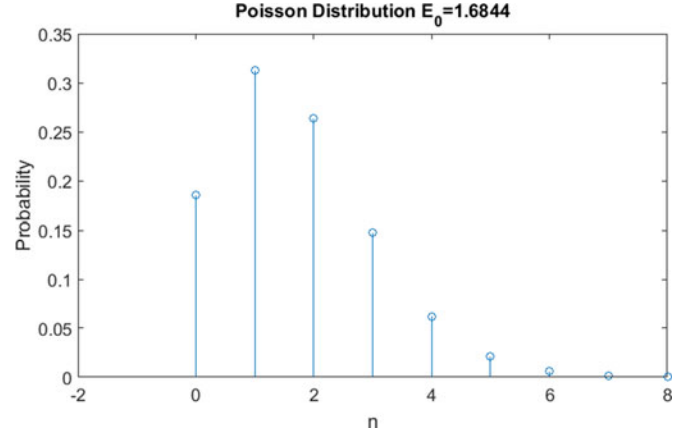
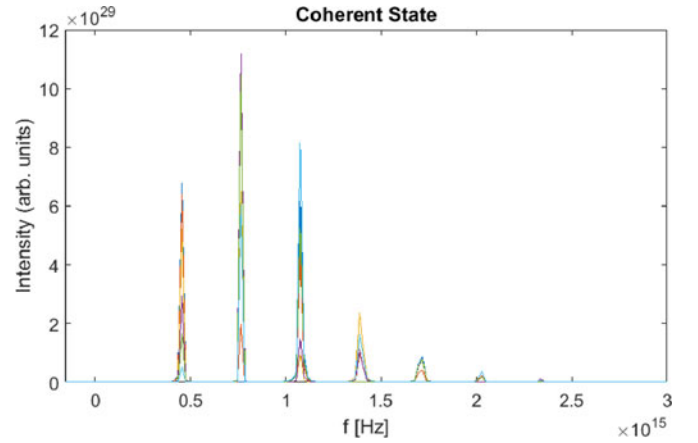

 Fig. 6. Plot of the Poisson distribution with $E_0 = 1.6844$ photons.


Fig. 7. Plot of eigenenergy levels of a simulated coherent state.

ous value. This expected Poisson distribution is plotted in Fig. 6. With 18 photons in the simulation space, the coherent state simulation result is plotted in Fig. 7. We can see that the simulated distribution of states closely resembles the predicted Poisson distribution.

V. CONCLUSION

In this paper, a new FDTD simulation scheme for the coupled Maxwell–Schrödinger system is presented. By directly using the potentials \mathbf{A} and Φ , approximations existing in the literature are avoided, and the computation made more efficient. The formulation is based on the first principle minimal coupling Hamiltonian. The only restriction is that of the semiclassical picture, which dictates the field to be in coherent states not entangled with the electron states. The calculations are numerically exact within this framework. This is unlike previous works in atom–field modeling where either the Jaynes–Cummings model is used, or the rotating wave approximation is made [24].

This paper portends well for future work where a fully quantized numerical model for field–atom system needs to be developed. It also allows the incorporation of field–atom effects in future quantum systems, such as density functional calculations, or more sophisticated $\mathbf{k} \cdot \mathbf{p}$ calculations in effective mass Schrödinger system. It is directly applicable in the study of quantum optics using quantum dots, or in nanoplasmonics, where the

quantum confinement of charges are important for their electromagnetic response. Also, the FDTD scheme is not costly for low-dimensional system, such as the popular quantum wells and quantum wires. Explicit time-domain simulations that allow the visualization of electron wavefunctions and field profiles will open up new understanding in these structures. Hence, the prowess of modern computers can be harnessed for the FDTD simulation scheme of the Maxwell–Schrödinger system which is a valid and useful tool in the study of nanostructures interacting with light.

APPENDIX A DISCRETE VECTOR CALCULUS

The discrete vector calculus forms the basis for the electromagnetic theory on a lattice. A brief overview is given on this topic. The paper [15] includes the details.

A differentiation can be approximated by a forward or backward difference. When $g(x) = \partial_x f(x)$

$$g_{m+1/2} = \tilde{\partial}_x f_m = \frac{f_{m+1} - f_m}{\Delta_x} \quad (19)$$

$$g_{m-1/2} = \hat{\partial}_x f_m = \frac{f_m - f_{m-1}}{\Delta_x} \quad (20)$$

where $\partial_x = \frac{\partial}{\partial x}$, $f_m = f(m\Delta_x)$, and Δ_x is the length of one cell. A discrete gradient also has forward and backward directions as given below when $\mathbf{g} = \nabla f$

$$\tilde{\mathbf{g}}_{\text{mnp}} = \tilde{\nabla} f_{\text{mnp}} = \hat{x}\tilde{\partial}_x f_{\text{mnp}} + \hat{y}\tilde{\partial}_y f_{\text{mnp}} + \hat{z}\tilde{\partial}_z f_{\text{mnp}} \quad (21)$$

$$\hat{\mathbf{g}}_{\text{mnp}} = \hat{\nabla} f_{\text{mnp}} = \hat{x}\hat{\partial}_x f_{\text{mnp}} + \hat{y}\hat{\partial}_y f_{\text{mnp}} + \hat{z}\hat{\partial}_z f_{\text{mnp}} \quad (22)$$

where $\hat{x}, \hat{y}, \hat{z}$ are unit vectors in x, y, z directions, $\tilde{\mathbf{g}}_{\text{mnp}}$ is a fore-vector emanating from point (m, n, p) to $(m + 1/2, n, p)$, $(m, n + 1/2, p)$, and $(m, n, p + 1/2)$, and $\hat{\mathbf{g}}_{\text{mnp}}$ is a back-vector located on points $(m - 1/2, n, p)$, $(m, n - 1/2, p)$, and $(m, n, p - 1/2)$ all pointing to (m, n, p) .

If we have a fore-vector $\tilde{\mathbf{F}}_{\text{mnp}} = \hat{x}f_{m+1/2,n,p}^x + \hat{y}f_{m,n+1/2,p}^y + \hat{z}f_{m,n,p+1/2}^z$, then we define a discrete divergence associated with point (m, n, p) such that

$$\begin{aligned} d_{\text{mnp}} &= \tilde{\nabla} \cdot \tilde{\mathbf{F}}_{\text{mnp}} \\ &= \hat{\partial}_x f_{m+1/2,n,p}^x + \hat{\partial}_y f_{m,n+1/2,p}^y + \hat{\partial}_z f_{m,n,p+1/2}^z. \end{aligned} \quad (23)$$

Similarly, the direction can be in the other way as $d_{\text{mnp}} = \hat{\nabla} \cdot \hat{\mathbf{F}}_{\text{mnp}}$.

The discrete curl is defined as in (24) are shown at the bottom of the page. Similarly, $\tilde{\mathbf{B}}_{m-1/2,n-1/2,p-1/2} = \hat{\nabla} \times \hat{\mathbf{F}}_{\text{mnp}}$ is possible.

With these definitions, the discretization of the \mathbf{A} - Φ equations can be carried out, and produces the (8) through (9) in Section II. Furthermore, when discretization in time is done, these can be rearranged into the time-stepping equations for the field and sources, given in (25)–(27),

$$\rho_{\text{m}}^n = \rho_{\text{m}}^{n-1} - \Delta t (\hat{\nabla} \cdot \tilde{\mathbf{J}}_{\text{m}}^{n-1/2}) \quad (25)$$

$$\Phi_{\text{m}}^{n+1} = 2\Phi_{\text{m}}^n - \Phi_{\text{m}}^{n-1} + \frac{\Delta t^2}{\mu_{\text{m}} \epsilon_{\text{m}}^2} \left(\hat{\nabla} \cdot \epsilon_{\text{m}} \tilde{\nabla} \Phi_{\text{m}}^n + \rho_{\text{m}}^n \right) \quad (26)$$

$$\begin{aligned} \tilde{\mathbf{A}}_{\text{m}}^{n+1/2} &= 2\tilde{\mathbf{A}}_{\text{m}}^{n-1/2} - \tilde{\mathbf{A}}_{\text{m}}^{n-3/2} \\ &+ \frac{\Delta t^2}{\epsilon_{\text{m}}} \left(-\hat{\nabla} \times \mu_{\text{m}+1/2}^{-1} \tilde{\nabla} \times \tilde{\mathbf{A}}_{\text{m}}^{n-1/2} \right. \\ &\quad \left. + \epsilon_{\text{m}} \tilde{\nabla} \mu_{\text{m}}^{-1} \epsilon_{\text{m}}^{-2} \hat{\nabla} \cdot \epsilon_{\text{m}} \tilde{\mathbf{A}}_{\text{m}}^{n-1/2} + \tilde{\mathbf{J}}_{\text{m}}^{n-1/2} \right). \end{aligned} \quad (27)$$

APPENDIX B PERFECTLY MATCHED LAYER

We implement PML following the coordinate stretching idea in [18]. To this end, modify (3) and (4) by replacing the ∇ operator with its stretched coordinate counterpart ∇_s , given by

$$\nabla_s = \hat{x} \frac{1}{s_x} \frac{\partial}{\partial t} + \hat{y} \frac{1}{s_y} \frac{\partial}{\partial t} + \hat{z} \frac{1}{s_z} \frac{\partial}{\partial t}. \quad (28)$$

It can be shown that the wave vector becomes $\mathbf{k}_s = \hat{x} \frac{k_x}{s_x} + \hat{y} \frac{k_y}{s_y} + \hat{z} \frac{k_z}{s_z}$, so if one of $s_x, s_y,$ or s_z is complex, the wave gets attenuated in the corresponding $x-, y-,$ or $z-$ direction. These coordinate stretching parameters are defined as

$$s_x = 1 + i \frac{\sigma_x}{\omega \epsilon} \quad s_y = 1 + i \frac{\sigma_y}{\omega \epsilon} \quad s_z = 1 + i \frac{\sigma_z}{\omega \epsilon}. \quad (29)$$

Substituting (3) into (28) and transforming to the frequency domain we produce three equations for the so-called split-fields, $\Phi_{s_x}, \Phi_{s_y}, \Phi_{s_z}$

$$\frac{1}{s_x} \frac{\partial}{\partial x} [\epsilon \nabla_s \Phi]_x + \epsilon^2 \mu \omega^2 \Phi_{s_x} = -\rho \quad (30)$$

$$\frac{1}{s_y} \frac{\partial}{\partial y} [\epsilon \nabla_s \Phi]_y + \epsilon^2 \mu \omega^2 \Phi_{s_y} = 0 \quad (31)$$

$$\frac{1}{s_z} \frac{\partial}{\partial z} [\epsilon \nabla_s \Phi]_z + \epsilon^2 \mu \omega^2 \Phi_{s_z} = 0. \quad (32)$$

$$\begin{aligned} \hat{\mathbf{B}}_{m+1/2,n+1/2,p+1/2} &= \tilde{\nabla} \times \tilde{\mathbf{F}}_{\text{mnp}} = \hat{x} \left(\frac{f_{m,n+1,p+1/2}^z - f_{m,n,p+1/2}^z}{\Delta y} - \frac{f_{m,n+1/2,p+1}^y - f_{m,n+1/2,p}^y}{\Delta z} \right) \\ &+ \hat{y} \left(\frac{f_{m+1/2,n,p+1}^x - f_{m+1/2,n,p}^x}{\Delta z} - \frac{f_{m+1,n,p+1/2}^z - f_{m,n,p+1/2}^z}{\Delta z} \right) \\ &+ \hat{z} \left(\frac{f_{m+1,n+1/2,p}^y - f_{m,n+1/2,p}^y}{\Delta x} - \frac{f_{m+1/2,n+1,p}^x - f_{m+1/2,n,p}^x}{\Delta y} \right) \end{aligned} \quad (24)$$

The choice of placing the source in the first equation of the above three is an arbitrary and inconsequential. Further substituting (29) into (30) and transforming back into the time domain gives

$$\left(\epsilon^2 \mu \frac{\partial^2}{\partial t^2} + \sigma_x \epsilon \mu \frac{\partial}{\partial t} \right) \Phi_{s_x} = \frac{\partial}{\partial x} [\epsilon \nabla_s \Phi]_x + \rho. \quad (33)$$

By turning the equation into a discrete one, the time-stepping equation can be found as follows:

$$\Phi_{s_x}^{n+1} = \frac{1}{\frac{\epsilon^2 \mu}{\Delta t^2} + \frac{\sigma_x \epsilon \mu}{2\Delta t}} \left(-\epsilon^2 \mu \frac{-2\Phi_{s_x}^n + \Phi_{s_x}^{n-1}}{\Delta t^2} + \sigma_x \epsilon \mu \frac{\Phi_{s_x}^{n-1}}{2\Delta t} + \hat{\partial}_x [\epsilon \tilde{\nabla}_s \Phi]_x^n + \rho^n \right). \quad (34)$$

The only remaining term to find is the third term in the parenthesis on the right-hand side. We can write

$$[\tilde{\nabla}_s \Phi]_x^n = \frac{1}{s_x} \tilde{\partial}_x \Phi^n \quad (35)$$

which becomes

$$\left(1 + i \frac{\sigma_x}{\omega \epsilon} \right) [\tilde{\nabla}_s \Phi]_x = \tilde{\partial}_x \Phi^n. \quad (36)$$

Transforming this into a time-domain equation yields

$$\begin{aligned} [\tilde{\nabla}_s \Phi]_x^n \left(i + \frac{1}{2}, j, k \right) + \frac{\sigma_x}{\epsilon} \left(\sum_{m=1}^{n-1} [\tilde{\nabla}_s \Phi]_x^m \left(i + \frac{1}{2}, j, k \right) + \frac{1}{2} [\tilde{\nabla}_s \Phi]_x^n \left(i + \frac{1}{2}, j, k \right) \right) \Delta t \\ = \frac{\Phi^n(i+1, j, k) - \Phi^n(i, j, k)}{\Delta x}. \end{aligned} \quad (37)$$

The summation in this equation is a discrete integral using the midpoint rule. When $\frac{i}{\omega}$ is transformed to an operator in the time-domain, it is written as [25]

$$\frac{i}{\omega} \leftrightarrow \int_0^t dt' \approx \sum_{m=0}^n \Delta t. \quad (38)$$

Equation (37) can be used to find $[\tilde{\nabla}_s \Phi]_x^n$ using Φ^n . After finding this term, it can be used to find

$$\hat{\partial}_x [\epsilon \tilde{\nabla}_s \Phi]_x^n = \frac{\epsilon(i + \frac{1}{2}, j, k) [\tilde{\nabla}_s \Phi]_x^n - \epsilon(i - \frac{1}{2}, j, k) [\tilde{\nabla}_s \Phi]_x^n}{\Delta x}. \quad (39)$$

The spatial coordinates of $[\tilde{\nabla}_s \Phi]$ terms follow the ones of ϵ 's multiplied to them. This concludes the derivation of coordinate stretching PML for the discrete Φ equation.

Next, we apply PML to the \mathbf{A} equation. Plug the following quantities:

$$\mathbf{H} = \mu^{-1} \nabla_s \times \mathbf{A} \quad (40)$$

and

$$f = \epsilon^{-2} \mu^{-1} \nabla_s \cdot \epsilon \mathbf{A} \quad (41)$$

into the coordinate stretched (4), we get

$$\nabla_s \times \mathbf{H} + \epsilon \frac{\partial^2}{\partial t^2} \mathbf{A} - \epsilon [\nabla_s f] = \mathbf{J}. \quad (42)$$

Consider the x -component of this equation. By converting this to the frequency-domain, applying (28), and taking the x -component, we find

$$\frac{1}{s_y} \frac{\partial H_z}{\partial y} - \frac{1}{s_z} \frac{\partial H_y}{\partial z} - \epsilon \omega^2 A_x - \epsilon [\nabla_s f]_x = J_x. \quad (43)$$

Substituting (29) into this and simplifying the expression yields

$$\begin{aligned} \left(-\omega^2 - i\omega \frac{\sigma_z}{\epsilon} \right) \left[\frac{\partial H_z}{\partial y} \right] + \left(\omega^2 + i\omega \frac{\sigma_y}{\epsilon} \right) \left[\frac{\partial H_y}{\partial z} \right] \\ + \left(\epsilon \omega^4 + i\omega^3 (\sigma_y + \sigma_z) - \omega^2 \frac{\sigma_y \sigma_z}{\epsilon} \right) A_x \\ + \left(\omega^2 \epsilon + i\omega (\sigma_y + \sigma_z) - \frac{\sigma_y \sigma_z}{\epsilon} \right) [\nabla_s f]_x \\ = -\omega^2 J_x. \end{aligned} \quad (44)$$

Converting this back to time-domain equation (46) shown at the bottom of next page.

$$\begin{aligned} \left(\frac{\partial^2}{\partial t^2} + \frac{\sigma_z}{\epsilon} \frac{\partial}{\partial t} \right) \left[\frac{\partial H_z}{\partial y} \right] + \left(-\frac{\partial^2}{\partial t^2} - \frac{\sigma_y}{\epsilon} \frac{\partial}{\partial t} \right) \left[\frac{\partial H_y}{\partial z} \right] \\ + \left(\epsilon \frac{\partial^4}{\partial t^4} + (\sigma_y + \sigma_z) \frac{\partial^3}{\partial t^3} + \frac{\sigma_y \sigma_z}{\epsilon} \frac{\partial^2}{\partial t^2} \right) A_x \\ + \left(-\epsilon \frac{\partial^2}{\partial t^2} - (\sigma_y + \sigma_z) \frac{\partial}{\partial t} - \frac{\sigma_y \sigma_z}{\epsilon} \right) [\nabla_s f]_x = \frac{\partial^2}{\partial t^2} J_x. \end{aligned} \quad (45)$$

Discretizing the above equation yields (46), as shown on the next page. This is essentially time-stepping \mathbf{A} equation with PML. equation (46) at the bottom of the next page

Going back to (40), we can substitute (29) and take the s_x -component to find

$$\frac{1}{s_x} \frac{\partial}{\partial x} \hat{x} \times \mathbf{A} = \mu \mathbf{H}_{s_x}. \quad (47)$$

The process is similar for s_y - and s_z -components, so it will not be repeated here. In the frequency-domain, this equation becomes

$$\frac{\partial}{\partial x} (\hat{z} A_y - \hat{y} A_z) = \left(\mu + i \frac{\sigma_x \mu}{\omega \epsilon} \right) \mathbf{H}_{s_x}. \quad (48)$$

Since this equation has two vector components, we can split them into two, each in z - and y -directions, and convert them into time-domain equations as follows:

$$\begin{aligned} \frac{A_y^{n-\frac{1}{2}}(i+1, j+\frac{1}{2}, k) - A_y^{n-\frac{1}{2}}(i, j+\frac{1}{2}, k)}{\Delta x} \\ = \mu H_{s_x, z}^{n-\frac{1}{2}} + \frac{\sigma_x \mu}{\epsilon} \left(\sum_{m=1}^{n-1} H_{s_x, z}^{m-\frac{1}{2}} + \frac{1}{2} H_{s_x, z}^{n-\frac{1}{2}} \right) \Delta t \end{aligned} \quad (49)$$

$$-\frac{A_z^{n-\frac{1}{2}}(i+1, j, k+\frac{1}{2}) - A_z^{n-\frac{1}{2}}(i, j, k+\frac{1}{2})}{\Delta x}$$

$$= \mu H_{s_x, y}^{n-\frac{1}{2}} + \frac{\sigma_x \mu}{\epsilon} \left(\sum_{m=1}^{n-1} H_{s_x, y}^{m-\frac{1}{2}} + \frac{1}{2} H_{s_x, y}^{n-\frac{1}{2}} \right) \Delta t. \quad (50)$$

$H_{s_x, z}^{n-\frac{1}{2}}$ can be calculated from $A_y^{n-\frac{1}{2}}$, and $H_{s_x, y}^{n-\frac{1}{2}}$ can be calculated from $A_z^{n-\frac{1}{2}}$. Once s_y - and s_z -components are also found from (40) in a similar manner, the magnetic field can be recovered as $H_x = H_{s_x, x} + H_{s_y, x} + H_{s_z, x}$ and same for H_y and H_z . From this, the partial derivatives of H terms in (46) can easily be found

$$\left[\frac{\partial H_z}{\partial y} \right] = \frac{H_z(i + \frac{1}{2}, j + \frac{1}{2}, k) - H_z(i + \frac{1}{2}, j - \frac{1}{2}, k)}{\Delta y} \quad (51)$$

$$\left[\frac{\partial H_y}{\partial z} \right] = \frac{H_y(i + \frac{1}{2}, j, k + \frac{1}{2}) - H_y(i + \frac{1}{2}, j, k - \frac{1}{2})}{\Delta z}. \quad (52)$$

The remaining term to be derived in (46) is the gradient of f term. In order to derive this, f must be derived first. We have the following relationship:

$$\mu \epsilon^2 f = \nabla_s \cdot \epsilon \mathbf{A}. \quad (53)$$

Applying the split-field method and taking the s_x -component of this equation

$$\left(1 + i \frac{\sigma_x}{\omega \epsilon}\right) f_{s_x} = \frac{1}{\mu \epsilon^2} \frac{\partial}{\partial x} (\epsilon A_x). \quad (54)$$

We convert this to time-domain and discretize it

$$\begin{aligned} f_{s_x}^{n-\frac{1}{2}} + \frac{\sigma_x}{\epsilon} \left(\sum_{m=1}^{n-1} f_{s_x}^{m-\frac{1}{2}} + \frac{1}{2} f_{s_x}^{n-\frac{1}{2}} \right) \Delta t \\ = \frac{1}{\mu \epsilon^2} \frac{\epsilon(i + \frac{1}{2}, j, k) A_x^{n-\frac{1}{2}} - \epsilon(i - \frac{1}{2}, j, k) A_x^{n-\frac{1}{2}}}{\Delta x}. \end{aligned} \quad (55)$$

Using this equation, $f_{s_x}^{n-\frac{1}{2}}$ can be found from $A_x^{n-\frac{1}{2}}$. The terms f_{s_y} and f_{s_z} can be found similarly, and then $f = f_{s_x} + f_{s_y} + f_{s_z}$. From this f term, the gradient of f can be calculated as follows:

$$\nabla_s f = [\nabla_s f]. \quad (56)$$

Taking the s_x -component of this

$$\frac{1}{s_x} \frac{\partial}{\partial x} \hat{x} f = [\nabla_s f]_{s_x} = [\nabla_s f]_x. \quad (57)$$

Note that the s_x -component in this case happens to be the x -component because the vector is only in the x -direction. The discretized time-domain version of this equation is

$$\begin{aligned} \frac{f^{n-\frac{1}{2}}(i+1, j, k) - f^{n-\frac{1}{2}}(i, j, k)}{\Delta x} \\ = [\nabla_s f]_x^{n-\frac{1}{2}} + \frac{\sigma_x}{\epsilon} \left(\sum_{m=1}^{n-1} [\nabla_s f]_x^{m-\frac{1}{2}} + \frac{1}{2} [\nabla_s f]_x^{n-\frac{1}{2}} \right) \Delta t. \end{aligned} \quad (58)$$

This concludes the derivation of the coordinate stretching PML for the \mathbf{A} - Φ equations.

APPENDIX C

DISCRETIZATION OF THE MAXWELL-SCHRÖDINGER EQUATIONS

The discrete version of the modified Schrödinger equation is very similar to the original one

$$\begin{aligned} i \hbar \hat{\partial}_t \psi_{\mathbf{m}}^n = \left[\frac{1}{2m^*} \left(\frac{\hbar}{i} \hat{\nabla} - q \tilde{\mathbf{A}}_{\mathbf{m}}^n \right) \cdot \left(\frac{\hbar}{i} \tilde{\nabla} - q \tilde{\mathbf{A}}_{\mathbf{m}}^n \right) \right. \\ \left. + q \Phi_{\mathbf{m}}^n + V_{\mathbf{m}} \right] \psi_{\mathbf{m}}^n. \end{aligned} \quad (59)$$

The time-stepping equation obtained from the above is

$$\begin{aligned} \psi_{\mathbf{m}}^{n+1} = \psi_{\mathbf{m}}^{n-1} + \frac{\Delta t}{m^*} \left[i \hbar \hat{\nabla} \cdot \tilde{\nabla} \psi_{\mathbf{m}}^n + q \hat{\nabla} \cdot (\tilde{\mathbf{A}}_{\mathbf{m}}^n \psi_{\mathbf{m}}^n) \right. \\ \left. + q \tilde{\mathbf{A}}_{\mathbf{m}}^n \cdot \tilde{\nabla} \psi_{\mathbf{m}}^n - i \frac{q^2 |\tilde{\mathbf{A}}_{\mathbf{m}}^n|^2}{\hbar} \psi_{\mathbf{m}}^n \right] - i \frac{2 \Delta t q \Phi_{\mathbf{m}}^n}{\hbar} \psi_{\mathbf{m}}^n \\ - i \frac{2 \Delta t V_{\mathbf{m}}}{\hbar} \psi_{\mathbf{m}}^n. \end{aligned} \quad (60)$$

The discretized expression for the second term on the right-hand side of the above equation has been derived in other papers such as [23]. The rest can be written down using the same discrete vector calculus method as given in Appendix A. It is worth noting that, whereas \mathbf{A} and ψ are not on the same grid, average values for ψ are used at the two nearby nodes.

$$\begin{aligned} \frac{\left[\frac{\partial H_z}{\partial y} \right]^{n-\frac{1}{2}} - 2 \left[\frac{\partial H_z}{\partial y} \right]^{n-\frac{3}{2}} + \left[\frac{\partial H_z}{\partial y} \right]^{n-\frac{5}{2}}}{\Delta t^2} + \frac{\sigma_z}{\epsilon} \frac{\left[\frac{\partial H_z}{\partial y} \right]^{n-\frac{1}{2}} - \left[\frac{\partial H_z}{\partial y} \right]^{n-\frac{5}{2}}}{2 \Delta t} - \frac{\left[\frac{\partial H_y}{\partial z} \right]^{n-\frac{1}{2}} - 2 \left[\frac{\partial H_y}{\partial z} \right]^{n-\frac{3}{2}} + \left[\frac{\partial H_y}{\partial z} \right]^{n-\frac{5}{2}}}{\Delta t^2} \\ - \frac{\sigma_y}{\epsilon} \frac{\left[\frac{\partial H_y}{\partial z} \right]^{n-\frac{1}{2}} - \left[\frac{\partial H_y}{\partial z} \right]^{n-\frac{5}{2}}}{2 \Delta t} + \epsilon \frac{A_x^{n+\frac{1}{2}} - 4 A_x^{n-\frac{1}{2}} + 6 A_x^{n-\frac{3}{2}} - 4 A_x^{n-\frac{5}{2}} + A_x^{n-\frac{7}{2}}}{\Delta t^4} \\ + (\sigma_y + \sigma_z) \frac{\frac{1}{2} A_x^{n+\frac{1}{2}} - A_x^{n-\frac{1}{2}} + A_x^{n-\frac{5}{2}} - \frac{1}{2} A_x^{n-\frac{7}{2}}}{\Delta t^3} + \frac{\sigma_y \sigma_z}{\epsilon} \frac{A_x^{n-\frac{1}{2}} - 2 A_x^{n-\frac{3}{2}} + A_x^{n-\frac{5}{2}}}{\Delta t^2} - \epsilon \frac{[\nabla_s f]_x^{n-\frac{1}{2}} - 2 [\nabla_s f]_x^{n-\frac{3}{2}} + [\nabla_s f]_x^{n-\frac{5}{2}}}{\Delta t^2} \\ - (\sigma_y + \sigma_z) \frac{[\nabla_s f]_x^{n-\frac{1}{2}} - [\nabla_s f]_x^{n-\frac{5}{2}}}{2 \Delta t} - \frac{\sigma_y \sigma_z}{\epsilon} [\nabla_s f]_x^{n-\frac{3}{2}} = \frac{J_x^{n-\frac{1}{2}} - 2 J_x^{n-\frac{3}{2}} + J_x^{n-\frac{5}{2}}}{\Delta t^2} \end{aligned} \quad (46)$$

The remaining equation to be discretized is the particle current equation. The discrete version of that is

$$\tilde{\mathbf{J}}_{q,\mathbf{m}}^{n+1/2} = \frac{q}{2} \left\{ \left[\frac{\frac{\hbar}{i} \tilde{\nabla} - q \tilde{\mathbf{A}}_{\mathbf{m}}^{n+1/2}}{m^*} \psi_{\mathbf{m}}^{n+1/2} \right]^* \psi_{\mathbf{m}}^{n+1/2} + (\psi_{\mathbf{m}}^{n+1/2})^* \left[\frac{\frac{\hbar}{i} \tilde{\nabla} - q \tilde{\mathbf{A}}_{\mathbf{m}}^{n+1/2}}{m^*} \psi_{\mathbf{m}}^{n+1/2} \right] \right\}. \quad (61)$$

This can be simplified as

$$\tilde{\mathbf{J}}_{q,\mathbf{m}}^{n+1/2} = -\frac{q}{m^*} \left[\text{Re} \{ i \hbar (\psi_{\mathbf{m}}^{n+1/2})^* \tilde{\nabla} \psi_{\mathbf{m}}^{n+1/2} \} + q |\psi_{\mathbf{m}}^{n+1/2}|^2 \tilde{\mathbf{A}}_{\mathbf{m}}^{n+1/2} \right]. \quad (62)$$

There are two terms in this equation, and the x -component of the discretized expression for the first terms looks like

$$[\psi_{\mathbf{m}}^* \tilde{\nabla} \psi_{\mathbf{m}}]_x = \frac{\psi^*(i+1, j, k) + \psi^*(i, j, k)}{2} \times \frac{\psi(i+1, j, k) - \psi(i, j, k)}{\Delta x}. \quad (63)$$

Only the real part of the above term enters into (62). The y - and z -components are analogous. For the x -component of the second term, we have

$$[|\psi_{\mathbf{m}}|^2 \tilde{\mathbf{A}}_{\mathbf{m}}]_x = \frac{\psi^2(i+1, j, k) + \psi^2(i, j, k)}{2} A_x \left(i + \frac{1}{2}, j, k \right). \quad (64)$$

The y - and z -components can be written analogously, and this completes the discretization for the Maxwell–Schrödinger system.

REFERENCES

- [1] M. O. Scully and M. S. Zubairy, *Quantum Optics*. Cambridge, U.K.: Cambridge Univ. Press, 2002.
- [2] R. W. Ziolkowski, “The incorporation of microscopic material models into the FDTD approach for ultrafast optical pulse simulations,” *IEEE Trans. Antennas Propag.*, vol. 45, no. 3, pp. 375–391, Mar. 1997.
- [3] S. Hellstrom and Y. Fu, “Dynamic optical response of an excitonic quantum dot studied by solving the self-consistent Maxwell–Schrödinger equations nonperturbatively,” *Phys. Rev. B, Condens. Matter*, vol. 82, 2010, Art. no. 245305.
- [4] A. Pusch, S. Wuestner, J. M. Hamm, K. L. Tsakmakidis, and O. Hess, “Coherent amplification and noise in gain-enhanced nanoplasmonic metamaterials: A Maxwell–Bloch Langevin approach,” *ACS Nano*, vol. 6, no. 3, pp. 2420–2431, 2012.
- [5] K. Lopata and D. Neuhauser, “Nonlinear nanopolaritonics: Finite-difference time-domain Maxwell–Schrödinger simulation of molecule-assisted plasmon transfer,” *J. Chem. Phys.*, vol. 131, 2009, Art. no. 014701.
- [6] K. Lopata and D. Neuhauser, “Multiscale Maxwell–Schrödinger modeling: A split field finite-difference time-domain approach to molecular nanopolaritonics,” *J. Chem. Phys.*, vol. 130, 2009, Art. no. 104707.
- [7] W. Sui, J. Yang, X. H. Yun, and C. Wang, “Including quantum effects in electromagnetic system—An FDTD solution to Maxwell–Schrödinger equations,” in *IEEE MTT-S Int. Microw. Symp. Dig.*, 2007, pp. 1979–1982.
- [8] T. Takeuchi, S. Ohnuki, and T. Sako, “Maxwell–Schrödinger hybrid simulation for optically controlling quantum states: A scheme for designing control pulses,” *Phys. Rev. A, Gen. Phys.*, vol. 91, no. 3, 2015, Art. no. 033401.
- [9] I. Ahmed, E. H. Khoo, E. Li, and R. Mittra, “A hybrid approach for solving coupled Maxwell and Schrödinger equations arising in the simulation of nano-devices,” *IEEE Antennas Wireless Propag. Lett.*, vol. 9, pp. 914–917, 2010.
- [10] S. Ohnuki, T. Takeuchi, T. Sako, Y. Ashizawa, K. Nakagawa, and M. Tanaka, “Coupled analysis of Maxwell–Schrödinger equations by using the length gauge: Harmonic model of a nanoplate subjected to a 2-D electromagnetic field,” *Int. J. Numer. Model. Electron. Netw. Devices Fields*, vol. 26, no. 6, pp. 533–544, 2013.
- [11] Y. Zeng, Y. Fu, M. Bengtsson, X. Chen, W. Lu, and H. Agren, “Finite-difference time-domain simulations of exciton-polariton resonances in quantum dot arrays,” *Opt. Exp.*, vol. 16, no. 7, pp. 4507–4519, 2008.
- [12] A. Bratovsky *et al.*, “A metal-wire/quantum-dot composite metamaterial with negative epsilon and compensated optical loss,” *Appl. Phys. Lett.*, vol. 93, 2008, Art. no. 193106.
- [13] J. M. Llorens, I. Prieto, L. E. Munioz-Camuniez, and P. A. Postigo, “Analysis of the strong coupling regime of a quantum well in a photonic crystal microcavity and its polarization dependence studied by the finite-difference time-domain method,” *J. Opt. Soc. Amer. B, Opt. Phys.*, vol. 30, no. 5, pp. 1222–1231, 2013.
- [14] W. C. Chew, “Vector potential electromagnetics with generalized gauge for inhomogeneous media: Formulation,” *Progr. Electromagn. Res.*, vol. 149, pp. 69–84, 2014.
- [15] W. C. Chew, “Electromagnetic theory on a lattice,” *J. Appl. Phys.*, vol. 75, no. 10, p. 4843, 1994.
- [16] K. S. Yee, “Numerical solution of initial boundary value problems involving Maxwell’s equations in isotropic media,” *IEEE Trans. Antennas Propag.*, vol. AP-14, no. 3, pp. 302–307, May 1966.
- [17] J.-M. Jin, *Theory and Computation of Electromagnetic Fields*. Hoboken, NJ, USA: Wiley, 2010.
- [18] W. C. Chew and W. H. Weedon, “A 3-D perfectly matched medium from modified Maxwell’s equations with stretched coordinates,” *Microw. Opt. Technol. Lett.*, vol. 7, no. 13, pp. 599–604, 1994.
- [19] R. Feynman, R. B. Leighton, and M. L. Sands, *The Feynman Lectures on Physics*. Reading, MA, USA: Addison-Wesley, 1965.
- [20] A. Soriano, E. A. Navarro, J. A. Portí, and V. Such, “Analysis of the finite difference time domain technique to solve the Schrödinger equation for quantum devices,” *J. Appl. Phys.*, vol. 95, no. 12, pp. 8011–8018, 2004.
- [21] R. J. Warburton, “Single spins in self-assembled quantum dots,” *Nature Mater.*, vol. 12, no. 6, pp. 483–493, 2013.
- [22] D. A. B. Miller, *Quantum Mechanics for Scientists and Engineers*. New York, NY, USA: Cambridge Univ. Press, 2008.
- [23] D. M. Sullivan and D. S. Citrin, “Determination of the eigenfunctions of arbitrary nanostructures using time domain simulation,” *J. Appl. Phys.*, vol. 91, no. 5, pp. 3219–3226, 2002.
- [24] C. C. Gerry and P. L. Knight, *Introductory Quantum Optics*. Cambridge, U.K.: Cambridge Univ. Press, 2008.
- [25] L. Zhao and A. C. Cangellaris, “GT-PML: Generalized theory of perfectly matched layers and its application to the reflectionless truncation of finite-difference time-domain grids,” *IEEE Trans. Microw. Theory Techn.*, vol. 44, no. 12, pp. 2555–2563, Dec. 1996.

Christopher J. Ryu, photograph and biography not available at the time of publication.

Aiyin Y. Liu, photograph and biography not available at the time of publication.

Wei E. I. Sha (M’09), photograph and biography not available at the time of publication.

Weng C. Chew (S’79–M’80–SM’86–F’93), photograph and biography not available at the time of publication.